Hindawi
International Journal of Aerospace Engineering
Volume 2022, Article ID 6447812, 15 pages
https://doi.org/10.1155/2022/6447812

Research Article

Fixed-Time Fault-Tolerant Tracking Control of Fixed-Wing UAVs with Actuator Fault and Unmatched Disturbances

Zhonghua Wu and Shuaipeng Zheng

School of Electrical Engineering and Automation, Henan Polytechnic University, Jiaozuo 454000, China

Correspondence should be addressed to Zhonghua Wu; wuzhonghua@hpu.edu.cn

Received 14 April 2022; Accepted 6 September 2022; Published 21 November 2022

Academic Editor: Hao Chen

This paper presents a dynamic surface fixed-time fault-tolerant control strategy for the longitudinal dynamic model of fixed-wing unmanned aerial vehicles (UAVs). Firstly, a novel disturbance observer is constructed to precisely estimate the lumped disturbance. Secondly, without fractional power terms in the designed fixed-time fault-tolerant controller, the potential singular value problem is tactfully avoided, which often exists in the stability analysis of the traditional fixed-time controller design. Thirdly, a novel fixed-time filter is proposed to overcome the phenomenon of "differential explosion" in the backstepping control scheme. Lyapunov stability analysis guarantees that the tracking errors can converge to the neighborhood of the origin in the fixed time. The simulation results verify the effectiveness of the proposed control scheme.

1. Introduction

Fixed-wing UAVs have played an essential role in high-risk and complex missions due to their flexibility and maneuverability [1]. The complex flight conditions make the UAVs subject to actuator fault during operation, which may degrade the stability and robustness of flight control systems, and even lead to a catastrophic accident, thus requiring to explore the fault-tolerant control (FTC) of UAVs. Many researchers have concentrated on addressing the control problem of fixed-wing UAVs subject to actuator fault, thereby publishing numerous results regarding passive or active FTC. Active FTC identifies faults through fault detection and diagnosis block in real time, while passive FTC uses a single fixed controller through the robust control strategy [2–5].

An adaptive control approach consisting of a radial base function neural network (RBFNN) was proposed for coaxial octorotor UAV subject to actuator faults [6]. By introducing a prescribed performance function on the synchronized tracking errors, the decentralized finite-time adaptive fault-tolerant synchronization tracking control scheme is proposed for multi-UAVs in the presence of actuator faults [7]. A distributed adaptive FTC scheme is proposed in virtual of a distributed sliding mode estimator and disturbance observers [8]. In the presence of actuator fault, the distributed fault-tolerant output regulation for heterogeneous linear multiagent systems is proposed using the distributed fixed-time observer and adaptive fault-tolerant controller [9]. A constrained control scheme based on model reference adaptive control is investigated for the longitudinal motion of a commercial aircraft with actuator faults and saturation nonlinearities [10]. By using the extended Kalman filter (EKF) to update the weighting parameters of the neural network (NN), a new online detection strategy is developed to detect faults in sensors and actuators of UAVs [11].

The external disturbance may degrade the flight performance of fixed-wing UAVs directly. Therefore, it is essential to construct a disturbance observer against its adverse effect. A disturbance observer combined with a time delay estimation is designed to weaken the influence caused by the unknown dynamic parameters in the actuator of the rehabilitation robot [12]. A novel fixed-time extended state observer is presented to estimate the state errors and the total disturbances in the presence of nonlinear couplings, uncertain parameters, and external disturbances [13]. A

disturbance observer is incorporated into the control structure to efficiently estimate the lumped disturbances, including modeling inaccuracies and external perturbations [14]. A fixed-time adaptive fast super-twisting disturbance observer is built to estimate the external disturbance, in which two tunable gains are adjusted in real time by an adaptive law [15]. The disturbance observers, as mentioned above, need to know the upper bound of the external disturbance, which may hinder its practical engineering applications.

Backstepping control schemes have been widely used in the control system design of fixed-wing UAVs. However, the repeated derivation of the virtual control law in the backstepping designs will largely increase the computational complexity, called the "differential explosion" phenomenon. By introducing a first-order filter to estimate the derivative of the virtual control laws, the dynamic surface control (DSC) scheme is first proposed in [16]. An observer-based fuzzy neural dynamic surface control is presented for a flexible-joint manipulator system with input saturation and unknown disturbance [17]. Moreover, a composite learning fixed-time DSC scheme is proposed for nonlinear strict feedback systems with parameter uncertainties [18]. A constrained adaptive DSC approach is presented for uncertain nonlinear systems subject to full-state constraints [19].

Unlike the traditional finite-time control schemes, the upper bound of convergence time is irrelevant to the initial conditions in the fixed-time control scheme, leading to its extensive applications in UAVs. By introducing a continuously differentiable switching function, an adaptive fixed-time control strategy is proposed for autonomous ship landing operations of UAVs [20]. Moreover, a fixed-time controller combined with the obstacle Lyapunov function is designed for a class of surface ship systems with output constraints [21]. Motivated by the practical requirements of high precision and faster convergence rate for an automatic carrier landing, a fixed-time nonlinear flight controller is presented [22]. Anti-saturation coordinated controller is designed [23], which can guarantee the safe distance constraint of each spacecraft in the process of completing the configuration reconstruction task in a specified time. Using a distributed fixed-time observer to estimate the states of the virtual leader, a fixed-time attitude coordinated control is investigated for multispacecraft systems with unknown external disturbance [24]. However, those mentioned above backstepping fixed-time controllers contain fractional power terms, which may encounter the singular problem caused by the repeated derivation of the virtual control law.

Inspired by recent results [25–27], a fixed-time fault-tolerant controller without fractional power terms is proposed for fixed-wing UAVs subject to actuator fault and external disturbances. The main contributions of this work are threefold:

(1) Different from the conventional fixed-time algorithm, a simple fixed-time fault-tolerant controller scheme without fractional power terms is proposed, which overcomes the potential singularity problem often encountered in fixed-time backstepping designs

(2) Unlike the traditional DSC schemes, this paper proposes a simple and smooth fixed-time filter in the control design, reducing the complexity of the control system and ensuring dynamic surface filter error to satisfy fixed-time convergence

(3) A new type of disturbance observer, with an adaptive term to estimate the upper bound of the lumped disturbance, is proposed, thus leading to an accurate estimation of the lumped disturbance

The layout of this paper is organized as follows. The problem formulation and preliminaries are introduced in Section 2. The construction of the new type of disturbance observer is described in Section 3. The fixed-time fault-tolerant controller and a new fixed-time dynamic surface filter are presented in Section 4. In Section 5, the numerical simulation indicates the effectiveness of the proposed control scheme, followed by the conclusions in Section 6.

2. Problem Formulation and Preliminaries

2.1. Model Description. The nonlinear longitudinal dynamic model of fixed-wing UAV is given as follows:

$$\begin{aligned} \dot{\gamma} &= \frac{L + T\sin\alpha}{m\mathrm{V}} - \frac{g}{V}\cos\gamma + \Delta_\gamma, \\ \dot{\alpha} &= q - \dot{\gamma} + \Delta_\alpha, \\ \dot{q} &= \frac{M}{I_{yy}} + \Delta_q, \end{aligned} \tag{1}$$

where γ, α and q are the flight-path angle, angle of attack, and pitch rate, respectively. m represents the mass of the UAV. g is the gravity acceleration, I_{yy} denotes the moment of inertia, $\Delta_\alpha, \Delta_\gamma, \Delta_q$ represent unknown external disturbances, and $T = T_{\max}\delta_T$ is the engine thrust.

The aerodynamic force and moment of the UAV are expressed as

$$\begin{aligned} L &= 0.5\rho V^2 \mathrm{S}C_L, \\ M &= 0.5\rho V^2 \mathrm{S}\mathrm{c}C_m, \end{aligned} \tag{2}$$

where ρ denotes the air density and S represents the wing platform area. C_L and C_m are the aerodynamic coefficients for drag force and pitch moment, respectively. The aerodynamic force and moment coefficients can be expressed as

$$\begin{aligned} C_L &= C_{L\alpha}\alpha + C_{L0}, \\ C_m &= C_{m\alpha}\alpha + C_{m0} + \frac{cq}{2V}C_{mq} + C_{m\delta_e}\delta_e, \end{aligned} \tag{3}$$

where $C_{L\alpha}, C_{L0}, C_{m\alpha}, C_{m0}, C_{mq}, C_{m\delta_e}$ represent the aerodynamic coefficients. δ_e is the actual elevator deflection.

2.2. Actuator Faults Model. To account for the actuator faults, the actual elevator deflection δ_e can be modeled as

$$\delta_e = p_1\delta_{e0} + b_{f1}, \tag{4}$$

where δ_{e0} denotes the designed elevator deflection and p_1 is the remaining control effectiveness factor with $0 < p_1 \le 1$. b_{f1} is the fault-bias factor.

2.3. System Transformation and Preparation. By substituting (2)–(4) into (1) and defining the state vector $[x_1 \quad x_2 \quad x_3]^T = [\gamma \quad \alpha \quad q]^T$, $u_0 = \delta_{e0}$, the longitudinal dynamics can be rewritten as

$$\begin{aligned} \dot{x}_1 &= f_1 + g_1x_2 + d_1, \\ \dot{x}_2 &= f_2 + g_2x_3 + d_2, \\ \dot{x}_3 &= f_3 + g_3u_0 + d_3, \end{aligned} \tag{5}$$

where

$$\begin{aligned} f_1 &= \frac{0.5\rho V^2 \mathrm{SC}_{L0}}{m\mathrm{V}} - \frac{g}{V}\cos\gamma, f_2 = -\dot{\gamma}, g_2 = 1, \\ g_1 &= \frac{0.5\rho V^2 \mathrm{SC}_{L\alpha} + T}{m\mathrm{V}}, g_3 = \frac{0.5\rho V^2 \mathrm{Sc}C_{m\delta_e}}{I_{\mathrm{yy}}}, \\ f_3 &= \frac{0.5\rho V^2 \mathrm{Sc}\left(C_{m\alpha}\alpha + C_{m0} + (\mathrm{cq}/2V)C_{m\mathrm{q}}\right)}{I_{\mathrm{yy}}}, \\ d_1 &= \Delta_\gamma, d_2 = \Delta_\alpha, d_3 = \Delta_q + g_3(p_1 - 1)\delta_{e0} + g_3b_{f1}. \end{aligned} \tag{6}$$

2.3.1. Control Objective. The control objective is to design a fixed-time fault-tolerant control scheme for the longitudinal dynamic model of fixed-wing UAVs subject to actuator fault and external disturbances, such that all the signals in the closed-loop system are bounded, and the reference signal tracking error converges to a small neighborhood of the origin in a fixed time.

Assumption 1. All states of the system (1) are measurable. Meanwhile, the reference trajectory γ_d is smoothly bounded and known.

Assumption 2. There exist unknown positive constants p_i such that $|d_i| \le p_i$ with $i = 1, 2, 3$.

Lemma 3. *[28] For a common dynamical system, $\dot{x}(t) = f(t, x)$ with $x(0) = 0$ and the origin be an equilibrium point, where $x \in R^n$ and $f : R_+ \times R^n \longrightarrow R^n$. Defining a Lyapunov candidate, $V(x) \ge 0$. If we can get that*

$$\dot{V}(x) \le -\mu_1 V(x)^\alpha - \mu_2 V(x)^\beta + C, \tag{7}$$

where μ_1, μ_2, α, and β are positive real numbers with $\alpha \in (0, 1)$, $\beta \in (1, \infty)$, then the origin $x = 0$ of the system is practical fixed-time stable, and the settling time function T_s can be estimated by

$$T_s \le \frac{1}{\mu_1(1-\alpha)} + \frac{1}{\mu_2(\beta-1)}. \tag{8}$$

Lemma 4. *[29] For any constant $\varepsilon > 0$ and any variable $x \in R$, the following inequality holds*

$$|x| - \frac{x^2}{\sqrt{x^2 + \varepsilon^2}} \le \varepsilon. \tag{9}$$

Lemma 5. *[26] For any positive real numbers $x_1, x_2, \cdots, x_n$ and $\alpha \in (0, 1)$, one has*

$$\left(\sum_{i=1}^{n} x_i\right)^\alpha \le \sum_{i=1}^{n} x_i^\alpha. \tag{10}$$

Lemma 6. *[30] If $x_i \ge 0$, $i = 1, \cdots, n$, then, the following inequality holds*

$$\left(\sum_{i=1}^{n} x_i\right)^2 \le n\sum_{i=1}^{n} x_i^2. \tag{11}$$

Lemma 7. *[21] For $x, y \in R$, Young's inequality holds*

$$xy \le \frac{\kappa^p}{p}|x|^p + \frac{1}{q\kappa^q}|y|^q, \tag{12}$$

where $\kappa > 0$, $p > 1$, $q > 1$, and $(p-1)(q-1) = 1$.

Lemma 8. *[19] For any constant $\delta > 0$ and any variable $x \in R$, the following inequality holds*

$$|x| - x\tanh\left(\frac{x}{\delta}\right) \le k\delta, \tag{13}$$

where k is a positive constant satisfying $k = e^{-(k+1)}$.

3. Disturbance Observer Design

In this section, a new type disturbance observer is proposed to eliminate the influence of the lumped disturbances.

3.1. Disturbance Observer Design. The disturbance observer is given as follows

$$\widehat{d}_i = \lambda_{i1}\pi_i + \lambda_{i2}\frac{\pi_i}{\sqrt{\pi^2 + (\varepsilon_i/\lambda_{i2})^2}} + \lambda_{i3}\pi_i^3 + \widehat{p}_i\tanh\left(\frac{\widehat{p}_i\pi_i}{\delta_i}\right), \tag{14}$$

where $\widehat{d}_i$ is the estimation of d_i and $\lambda_{i1}, \lambda_{i2}, \lambda_{i3}, \delta_i, \varepsilon_i$ are positive constants, $i = 1, 2, 3$. $\widehat{p}_i$ denotes the estimated value of the upper bound of the external unmatched disturbance signal. π_i is the auxiliary state of the disturbance observer,

which is governed by

$$\begin{aligned} \pi_i &= x_i - s_i, \\ \dot{s}_i &= \lambda_{i1}\pi_i + \lambda_{i2}\frac{\pi_i}{\sqrt{\pi^2 + (\varepsilon_i/\lambda_{i2})^2}} + \lambda_{i3}\pi_i^3 \\ &\quad + \widehat{p}_i \tanh\left(\frac{\widehat{p}_i\pi_i}{\delta_i}\right) + g_i x_{i+1} + f_i. \end{aligned} \tag{15}$$

$\widehat{p}_i$ can be calculated as

$$\dot{\widehat{p}}_i = |\pi_i| - \frac{\sigma_{1i}}{n_i}\widehat{p}_i - \frac{\sigma_{2i}}{n_i^2}\widehat{p}_i^3, \tag{16}$$

where $\sigma_{1i}, \sigma_{2i}, n_i$ are positive constants, $\tilde{p}_i = p_i - \widehat{p}_i$.

Defining the disturbance observer estimation error, $\tilde{d}_i = d_i - \widehat{d}_i$. Then, the derivative of π_i with respect to time can be written as

$$\dot{\pi}_i = d_i - \dot{\widehat{d}}_i = \dot{\tilde{d}}_i. \tag{17}$$

Remark 9. The disturbance observer design presented in [31] requires the upper bound of the external unmatched disturbance in advance, while the proposed disturbance observer releases this restrictive condition. Instead of using the sign function in the disturbance observer design [31], an adaptive term $\widehat{p}_i \tanh(\widehat{p}_i\pi_i/\delta_i)$ is introducing in the proposed novel disturbance observer, which successfully eliminates the chattering phenomenon.

3.2. Stability Analysis

Theorem 10. *Consider system (5), and assume that Assumptions 1 and 2 hold. If the disturbance observer is designed as (14) and there exist positive constants $\lambda_{i1}, \lambda_{i2}, \lambda_{i3}, \delta_i, \varepsilon_i, \sigma_{1i}, \sigma_{2i}, n_i$ for $i = 1, 2, 3$, then the estimated error $\tilde{p}_i$ and auxiliary state π_i converge to sets $\Omega_{\tilde{p}_i} = \{\tilde{p}_i \le \sqrt{2\sqrt{M/\mu_2}}\}, \Omega_{\pi_i} = \{\pi_i \le \sqrt{2\sqrt{M/\mu_2}}\}$ in a fixed time $T_d \le 2/\mu_1 + 1/\mu_2$, respectively.*

Proof. Consider the Lyapunov function candidate as

$$V_d = \sum_{i=1}^{3}\left(\frac{1}{2}\pi_i^2 + \frac{1}{2}\tilde{p}_i^2\right). \tag{18}$$

Then, it can be found that

$$\begin{aligned} \dot{V}_d &= \sum_{i=1}^{3}\pi_i\dot{\pi}_i + \tilde{p}_i\dot{\tilde{p}}_i, \\ &= \sum_{i=1}^{3}\left[\pi_i d_i - \lambda_{i1}\pi_i^2 - \lambda_{i2}\frac{\pi_i^2}{\sqrt{\pi^2 + (\varepsilon_i/\lambda_{i2})^2}} - \lambda_{i3}\pi_i^4\right. \\ &\quad - \widehat{p}_i\pi_i \tanh\left(\frac{\widehat{p}_i\pi_i}{\delta_i}\right) + \widehat{p}_i|\pi_i| - p_i|\pi_i| \\ &\quad \left. + \frac{\sigma_{1i}}{n_i}\tilde{p}_i\widehat{p}_i + \frac{\sigma_{2i}}{n_i^2}\tilde{p}_i\widehat{p}_i^3\right]. \end{aligned} \tag{19}$$

According to Lemma 4, we have

$$-\lambda_{i2}\frac{\pi_i^2}{\sqrt{\pi^2 + (\varepsilon_i/\lambda_{i2})^2}} \le -\lambda_{i2}|\pi_i| + \varepsilon_i. \tag{20}$$

Relying on Lemma 7, one gets

$$\pi_i d_i \le \lambda_{i1}\pi_i^2 + \frac{1}{4\lambda_{i1}}d_i^2. \tag{21}$$

From Lemma 8, we get

$$\widehat{p}_i|\pi_i| - \widehat{p}_i\pi_i \tanh\left(\frac{\widehat{p}_i\pi_i}{\delta_i}\right) \le |\widehat{p}_i\pi_i| - \widehat{p}_i\pi_i \tanh\left(\frac{\widehat{p}_i\pi_i}{\delta_i}\right) \le k\delta_i. \tag{22}$$

With regard to the terms $(\sigma_{1i}/n_i)\tilde{p}_i\widehat{p}_i$ and $(\sigma_{2i}/n_i^2)\tilde{p}_i\widehat{p}_i^3$ in (19), one can find that

$$\begin{aligned} \frac{\sigma_{1i}}{n_i}\tilde{p}_i\widehat{p}_i &= \frac{\sigma_{1i}}{n_i}\left(\tilde{p}_i p_i - \tilde{p}_i^2\right) + \frac{\sigma_{1i}\gamma_i}{\sqrt{2n_i}}\tilde{p}_i - \frac{\sigma_{1i}\gamma_i}{\sqrt{2n_i}}\tilde{p}_i \\ &\le \frac{\sigma_{1i}}{n_i}\left(\frac{1}{2}\tilde{p}_i^2 + \frac{1}{2}p_i^2 - \tilde{p}_i^2\right) + \frac{\sigma_{1i}}{2n_i}\tilde{p}_i^2 + \frac{\sigma_{1i}\gamma_i^2}{4} - \frac{\sigma_{1i}\gamma_i}{\sqrt{2n_i}}\tilde{p}_i, \end{aligned} \tag{23}$$

$$\begin{aligned} \frac{\sigma_{2i}}{n_i^2}\tilde{p}_i\widehat{p}_i^3 &= \frac{\sigma_{2i}}{n_i^2}\left(-\tilde{p}_i^4 - 3\tilde{p}_i^2 p_i^2 + \tilde{p}_i p_i^3 + 3p_i\tilde{p}_i^3\right) \\ &\le \frac{\sigma_{2i}}{n_i^2}\left(-\tilde{p}_i^4 - 3\tilde{p}_i^2 p_i^2 + \frac{3\theta_i^{4/3}}{4}\left|p_i^3\right|^{4/3}\right. \\ &\quad \left. + \frac{1}{4\theta_i^4}\tilde{p}_i^4 + 3p_i^2\tilde{p}_i^2 + \frac{3}{4}\tilde{p}_i^4\right), \end{aligned} \tag{24}$$

where $\gamma_i\theta_i$ are two positive constants.

□

Substituting (20), (21), (22), (23), and (24) into the derivative of V_d results in

$$\dot{V}_d \le \sum_{i=1}^{3}\left[-\sqrt{2}\lambda_{i2}\left(\frac{1}{2}\pi_i^2\right)^{1/2} - 4\lambda_{i3}\left(\frac{1}{2}\pi_i^2\right)^2 - \frac{\sigma_{2i}\left(\theta_i^4-1\right)}{\theta_i^4 n_i^2}\left(\frac{1}{2}\tilde{p}_i^2\right)^2 - \frac{\sigma_{1i}\gamma_i}{\sqrt{n_i}}\left(\frac{1}{2}\tilde{p}_i^2\right)^{1/2}\right] + M, \tag{25}$$

where $M = \sum_{i=1}^{3}[\varepsilon_i + k\delta_i + (3\sigma_{2i}\theta_i^{4/3}/4n_i^2)|p_i^3|^{4/3} + (\sigma_{1i}\gamma_i^2/4) + ((\sigma_{1i}/2n_i) + (1/4\lambda_{i1}))p_i^2]$.

Then, one has

$$\dot{V}_d \le -\mu_1 V_d^{1/2} - \mu_2 V_d^2 + M \le 0. \tag{26}$$

According to the above analysis, if $V_d \ge \sqrt{M/\mu_2}$, then $\dot{V}_d \le -\mu_1 {V_d}^{1/2} \le 0$, we can have that V_d will converge to the set $\{V_d : V_d \le \sqrt{M/\mu_2}\}$ in a fixed-time $T_d \le 2/\mu_1 + 1/\mu_2$, and thus, estimated error $\tilde{p}_i$ and auxiliary states π_i are uniformly ultimately bounded in a fixed time $T_d \le 2/\mu_1 + 1/\mu_2$.

4. Controller Design

In this section, a fixed-time fault-tolerant controller without fractional power terms scheme is proposed to eliminate the singular value problem for a fixed-wing UAV against actuator fault. To prevent the phenomenon of "differential explosion," a new fixed-time dynamic surface filter is added in the backstepping design.

4.1. Fixed-Time Controller and Filter Design. The tracking errors are defined as

$$\begin{aligned} z_1 &= x_1 - x_{1c}, \\ z_2 &= x_2 - x_{2c}, \\ z_3 &= x_3 - x_{3c}, \end{aligned} \tag{27}$$

where z_i is the tracking error, and x_{ic} is the fixed-time filter output signal, $i = 1, 2, 3$, $\gamma_d = x_{1c}$.

The filter errors are defined as

$$\begin{aligned} y_2 &= x_{2c} - x_{2d}, \\ y_3 &= x_{3c} - x_{3d}, \end{aligned} \tag{28}$$

where x_{id} is the virtual control signal and y_i is the error of x_{ic}, x_{id} with $y_i(0) = 0$, $i = 2, 3$.

Step 1. According to (27) and (28), we have

$$\dot{z}_1 = g_1(z_2 + y_2 + x_{2d}) + f_1 + d_1 - \dot{x}_{1c}. \tag{29}$$

The virtual control signal is designed as

$$x_{2d} = \frac{1}{g_1}\left[-f_1 - \hat{d}_1 - k_{11}\frac{z_1}{\sqrt{z_1^2 + (\varepsilon_{z1}/k_{11})^2}} - k_{12}z_1^3 - \left(\frac{k_{13}}{2} + \frac{g_1^2}{2k_{f23}}\right)z_1 + \dot{x}_{1c}\right], \tag{30}$$

where $k_{11}, k_{12}, k_{13}, k_{f23}, \varepsilon_{z1}$ are positive constants.

Remark 11. Different from the conventional fixed-time algorithm with fractional power terms presented in [22], the proposed fixed-time controllers do not contain fractional power terms, which overcome the potential singularity problem often caused by the repeated derivation of the virtual control law in fixed-time backstepping designs.

The Lyapunov function candidate is considered to be

$$V_1 = \frac{1}{2}z_1^2. \tag{31}$$

The time derivative of V_1 can be represented as

$$\dot{V}_1 = z_1\tilde{d}_1 - k_{11}\frac{z_1^2}{\sqrt{z_1^2 + (\varepsilon_{z1}/k_{11})^2}} - k_{12}z_1^4 - \left(\frac{k_{13}}{2} + \frac{g_1^2}{2k_{f23}}\right)z_1^2 + z_1z_2g_1 + z_1g_1y_2. \tag{32}$$

By applying Young's inequality and Lemma 4, one has

$$\begin{aligned} z_1\tilde{d}_1 &\le \frac{k_{13}z_1^2}{2} + \frac{1}{2k_{13}}\tilde{d}_1^2, \\ -k_{11}\frac{z_1^2}{\sqrt{z_1^2 + (\varepsilon_{z1}/k_{11})^2}} &\le -k_{11}|z_1| + \varepsilon_{z1}, \\ z_1g_1y_2 &\le \frac{g_1^2}{2k_{f23}}z_1^2 + \frac{k_{f23}}{2}y_2^2. \end{aligned} \tag{33}$$

Then, one has

$$\dot{V}_1 \le \frac{1}{2k_{13}}\tilde{d}_1^2 - k_{11}|z_1| + \varepsilon_{z1} - k_{12}z_1^4 + z_1z_2g_1 + \frac{k_{f23}}{2}y_2^2. \tag{34}$$

Step 2. Using (27) and (28), we have

$$\dot{z}_2 = g_2(z_3 + y_3 + x_{3d}) + f_2 + d_2 - \dot{x}_{2c}. \tag{35}$$

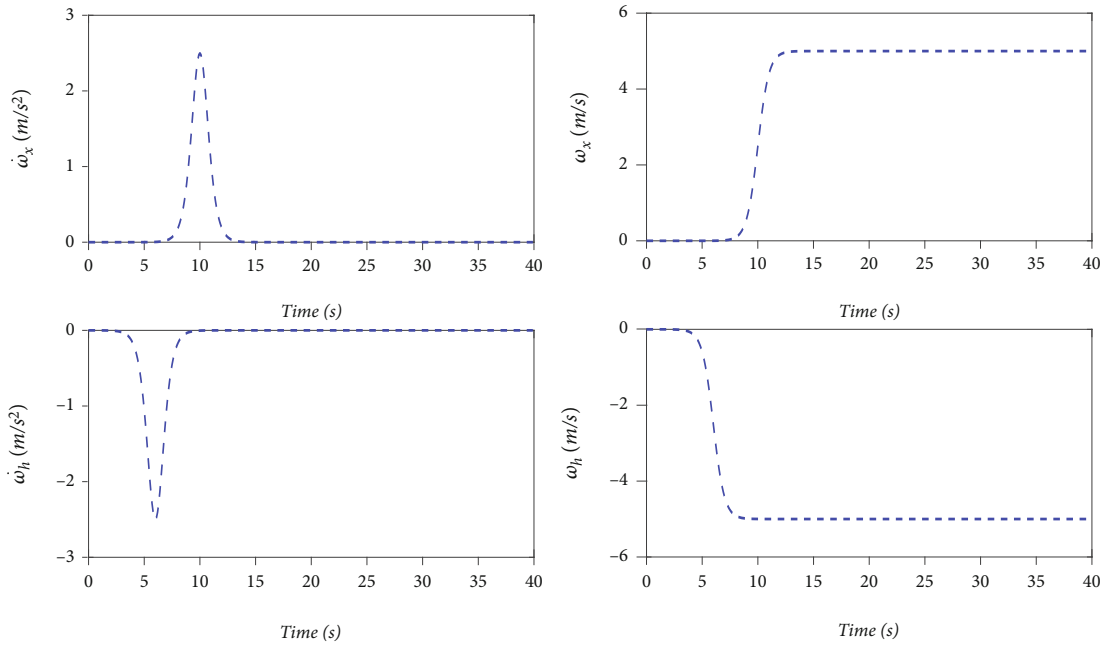

Figure 1: The curves of wind disturbance.

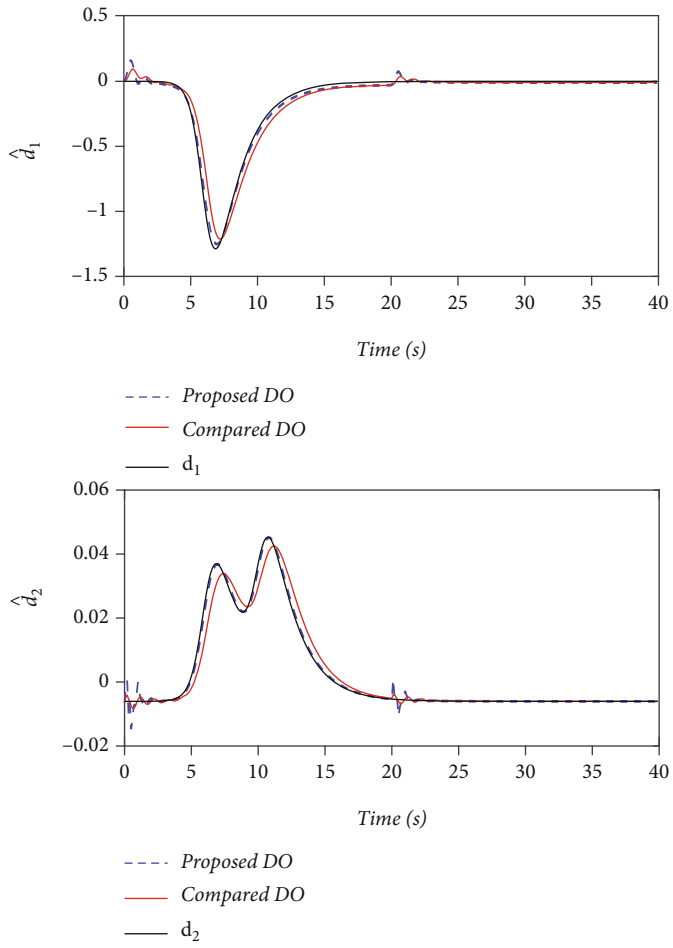

Figure 2: Estimation of d_1 and d_2.

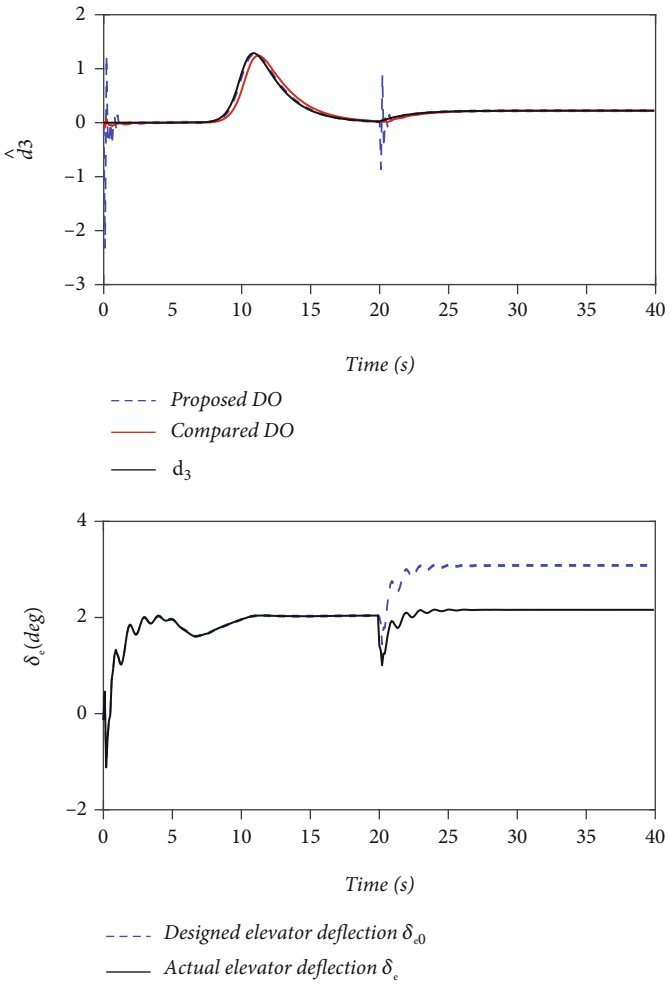

Figure 3: Estimation of d_3 and control input.

The virtual control signal is designed as

$$x_{3d} = \frac{1}{g_2}\left[-f_2 - \hat{d}_2 - k_{21}\frac{z_2}{\sqrt{z_2^2 + (\varepsilon_{z2}/k_{21})^2}} - k_{22}z_2^3 - \left(\frac{k_{23}}{2} + \frac{g_2^2}{2k_{f33}}\right)z_2 + \dot{x}_{2c} - g_1 z_1\right], \tag{36}$$

where $k_{21}, k_{22}, k_{23}, k_{f33}, \varepsilon_{z2}$ are positive constants.

The fixed-time filter is designed as

$$\dot{x}_{2c} = -k_{f21}\frac{y_2}{\sqrt{y_2^2 + (\varepsilon_{y2}/k_{f21})^2}} - k_{f22}y_2^3 - k_{f23}y_2, \tag{37}$$

where $k_{f21}, k_{f22}, k_{f23}, \varepsilon_{y2}$ are positive constants.

The Lyapunov function candidate is considered as

$$V_2 = \frac{1}{2}z_2^2 + \frac{1}{2}y_2^2. \tag{38}$$

The time derivative of V_2 can be represented as

$$\begin{aligned}\dot{V}_2 = {} & z_2\tilde{d}_2 - k_{21}\frac{z_2^2}{\sqrt{z_2^2 + (\varepsilon_{z2}/k_{21})^2}} - k_{22}z_2^4 \\ & - \left(\frac{k_{23}}{2} + \frac{g_2^2}{2k_{f33}}\right)z_2^2 - z_1 z_2 g_1 + z_2 z_3 g_2 \\ & + z_2 g_2 y_3 - k_{f21}\frac{y_2^2}{\sqrt{y_2^2 + (\varepsilon_{y2}/k_{f21})^2}} \\ & - k_{f22}y_2^4 - k_{f23}y_2^2 - \dot{x}_{2d}y_2.\end{aligned} \tag{39}$$

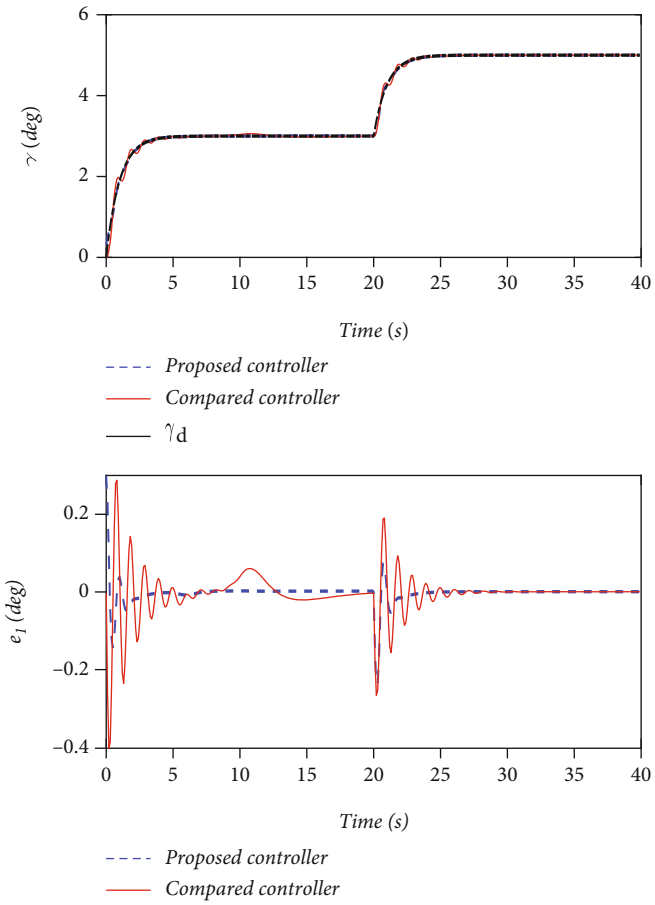

Figure 4: Tracking error e_1 and the trajectory of γ.

By applying Young's inequality and Lemma 4, we have

$$\begin{aligned} z_2\tilde{d}_2 &\le \frac{k_{23}}{2}z_2^2 + \frac{1}{2k_{23}}\tilde{d}_2^2, -k_{21}\frac{z_2^2}{\sqrt{z_2^2 + (\varepsilon_{z2}/k_{21})^2}} \\ &\le -k_{21}|z_2| + \varepsilon_{z2}, -k_{f21}\frac{y_2^2}{\sqrt{y_2^2 + (\varepsilon_{y2}/k_{f21})^2}} \\ &\le -k_{f21}|y_2| + \varepsilon_{y2}, \\ z_2 g_2 y_3 &\le \frac{g_2^2}{2k_{f33}}z_2^2 + \frac{k_{f33}}{2}y_3^2. \end{aligned} \tag{40}$$

Then, one has

$$\begin{aligned} \dot{V}_2 \le{}& \frac{1}{2k_{23}}\tilde{d}_2^2 - k_{21}|z_2| + \varepsilon_{z2} - k_{22}z_2^4 - z_1 z_2 g_1 \\ &+ z_2 z_3 g_2 - k_{f21}|y_2| + \varepsilon_{y2} - k_{f22}y_2^4 - k_{f23}y_2^2 \\ &+ \frac{k_{f33}}{2}y_3^2 - \dot{x}_{2d}y_2. \end{aligned} \tag{41}$$

Step 3. According to (27) and (28), we have

$$\dot{z}_3 = g_3 u_0 + f_3 + d_3 - \dot{x}_{3c}. \tag{42}$$

The virtual control signal is designed as

$$u_0 = \frac{1}{g_3}\left[-f_3 - \hat{d}_3 - k_{31}\frac{z_3}{\sqrt{z_3^2 + (\varepsilon_{z3}/k_{31})^2}} - k_{32}z_3^3 - k_{33}z_3 + \dot{x}_{3c} - g_2 z_2\right], \tag{43}$$

where $k_{31}, k_{32}, k_{33}, \varepsilon_{z3}$ are positive constants.

The fixed-time filter is designed as

$$\dot{x}_{3c} = -k_{f31}\frac{y_3}{\sqrt{y_3^2 + (\varepsilon_{y3}/k_{f31})^2}} - k_{f32}y_3^3 - k_{f33}y_3, \tag{44}$$

where $k_{f31}, k_{f32}, k_{f33}, \varepsilon_{y3}$ are positive constants.

Consider the following Lyapunov function candidate

$$V_3 = \frac{1}{2}z_3^2 + \frac{1}{2}y_3^2. \tag{45}$$

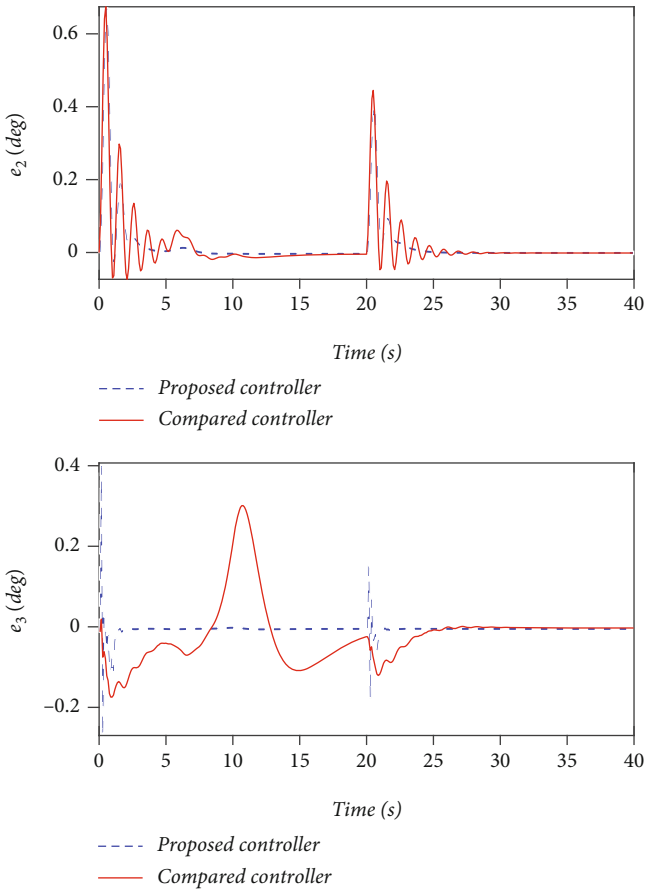

FIGURE 5: Tracking errors e_2 and e_3.

The time derivative of V_3 can be represented as

$$\begin{aligned}\dot{V}_3 = {} & z_3\tilde{d}_3 - k_{31}\frac{z_3^2}{\sqrt{z_3^2 + (\varepsilon_{z3}/k_{31})^2}} - k_{32}z_3^4 - k_{33}z_3^2 \\ & - z_2z_3g_2 - k_{f31}\frac{y_3^2}{\sqrt{y_3^2 + (\varepsilon_{y3}/k_{f31})^2}} - k_{f32}y_3^4 \\ & - k_{f33}y_3^2 - \dot{x}_{3d}y_3.\end{aligned} \tag{46}$$

Similar to the analysis of (33), (40), one has

$$\begin{aligned}\dot{V}_3 \le {} & \frac{1}{4k_{33}}\tilde{d}_3^2 - k_{31}|z_3| + \varepsilon_{z3} - k_{32}z_3^4 - z_2z_3g_2 \\ & - k_{f31}|y_3| + \varepsilon_{y3} - k_{f32}y_3^4 - k_{f33}y_3^2 - \dot{x}_{3d}y_3.\end{aligned} \tag{47}$$

4.2. Stability Analysis

Theorem 12. *Consider system (5), and assume that Assumptions 1 and 2 hold. The disturbance observer is designed as (14). The fixed-time controller is built as (30), (36), and (43), and dynamic filter is constructed as (37) and (44). For a given constant $P_1 > 0$, if $V(0) \le P_1$ and there exist the following positive constants $k_{i1}, k_{i2}, k_{i3}, \varepsilon_{zi}, \sigma_{1i}, \sigma_{2i}, n_i, \lambda_{i1}, \lambda_{i2}, \lambda_{i3}, \delta_i, \varepsilon_i, \theta_i, \gamma_i$ for $i = 1, 2, 3$ and $k_{fi1}, k_{fi2}, k_{fi3}, \varepsilon_{yi}$ for $i = 2, 3$, then, reference signal tracking errors z_i and fixed-time filter errors y_i converge to the neighborhood near the origin $\Omega_{z_i} = \{z_i \le \sqrt{2\sqrt{C/\mu_4}}\}, \Omega_{y_i} = \{y_i \le \sqrt{2\sqrt{C/\mu_4}}\}$ in a fixed time $T_s \le 2/\mu_3 + 1/\mu_4$.*

Remark 13. By differentiating x_{2d}, x_{3d}, one can obtain

$$\begin{aligned}\dot{x}_{2d} = {} & -\frac{\partial x_{2d}}{\partial f_1}\dot{f}_1 - \frac{\partial x_{2d}}{\partial \hat{d}_1}\dot{\hat{d}}_1 - \frac{\partial x_{2d}}{\partial z_1}\dot{z}_1 - \frac{\partial x_{2d}}{\partial y_2}\dot{y}_2 \\ & + \frac{\partial x_{2d}}{\partial g_1}\dot{g}_1 + \frac{\partial x_{2d}}{\partial \dot{x}_{1c}}\ddot{x}_{1c}, \\ \dot{x}_{3d} = {} & -\frac{\partial x_{3d}}{\partial f_2}\dot{f}_2 - \frac{\partial x_{3d}}{\partial \hat{d}_2}\dot{\hat{d}}_2 - \frac{\partial x_{3d}}{\partial z_2}\dot{z}_2 - \frac{\partial x_{2d}}{\partial z_1}\dot{z}_1 \\ & - \frac{\partial x_{3d}}{\partial y_3}\dot{y}_3 + \frac{\partial x_{2d}}{\partial g_1}\dot{g}_1 + \frac{\partial x_{2d}}{\partial g_2}\dot{g}_2 + \frac{\partial x_{3d}}{\partial \dot{x}_{2c}}\ddot{x}_{2c}.\end{aligned} \tag{48}$$

Because each partial of $\dot{x}_{2d}$ and $\dot{x}_{3d}$ is a continuous on a compact set $\Omega_V \times \Omega_{V_d}$, it has

$$-\dot{x}_{\mathrm{id}}y_i \le |\dot{x}_{\mathrm{id}}y_i| \le \frac{k_{\mathrm{fi}3}y_i^2}{2} + \frac{\bar{M}_{\mathrm{id}}^2}{2k_{\mathrm{fi}3}}, \tag{49}$$

2, 3.

Proof. The Lyapunov function candidate is considered to be

$$V = \sum_{i=1}^{3} V_i. \tag{50}$$

□

The time derivative of V can be represented as

$$\begin{aligned}\dot{V} = {} & \sum_{i=1}^{3} z_i\dot{z}_i + \sum_{i=2}^{3} y_i\dot{y}_i \\ \le {} & \sum_{i=1}^{3}\left(-\sqrt{2}k_{i1}\left(\frac{1}{2}z_i^2\right)^{1/2} - 4k_{i2}\left(\frac{1}{2}z_i^2\right)^2\right) \\ & + \sum_{i=2}^{3}\left(-\sqrt{2}k_{fi1}\left(\frac{1}{2}y_i^2\right)^{1/2} - 4k_{fi2}\left(\frac{1}{2}y_i^2\right)^2\right) + C\end{aligned} \tag{51}$$

where $C = \sum_{i=1}^{3}((1/2k_{i3})\tilde{d}_i^2 - (1/4k_{33})\tilde{d}_3^2 + \varepsilon_{\mathrm{zi}}) + \sum_{i=2}^{3}(\varepsilon_{yi} + (\bar{M}_{\mathrm{id}}^2/2k_{\mathrm{fi}3}))$.

Equation (51) can be further transformed as

$$\dot{V} \le -\mu_3V^{1/2} - \mu_4V^2 + C, \tag{52}$$

where μ_3 and μ_4 can be expressed as $\mu_3 = \min\{\sqrt{2}k_{11}, \sqrt{2}k_{i1}, \sqrt{2}k_{fi1}\}, \mu_4 = \min\{4k_{12}, 4k_{i2}, 4k_{fi2}\}, i = 2, 3$.

Note that, from (52), if $V \ge \sqrt{C/\mu_4}$, then $\dot{V} \le -\mu_3V^{1/2} \le 0$, which validates the boundedness of V. The boundedness of V means the boundedness of z_i for $i = 1, 2, 3$ and y_i for $i = 2, 3$.

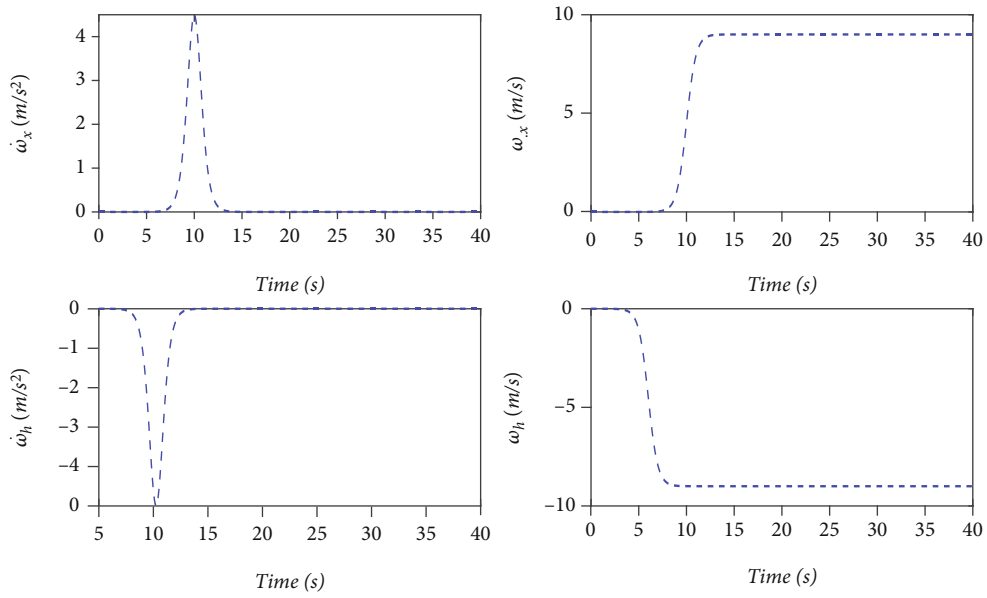

Figure 6: The curves of wind disturbance.

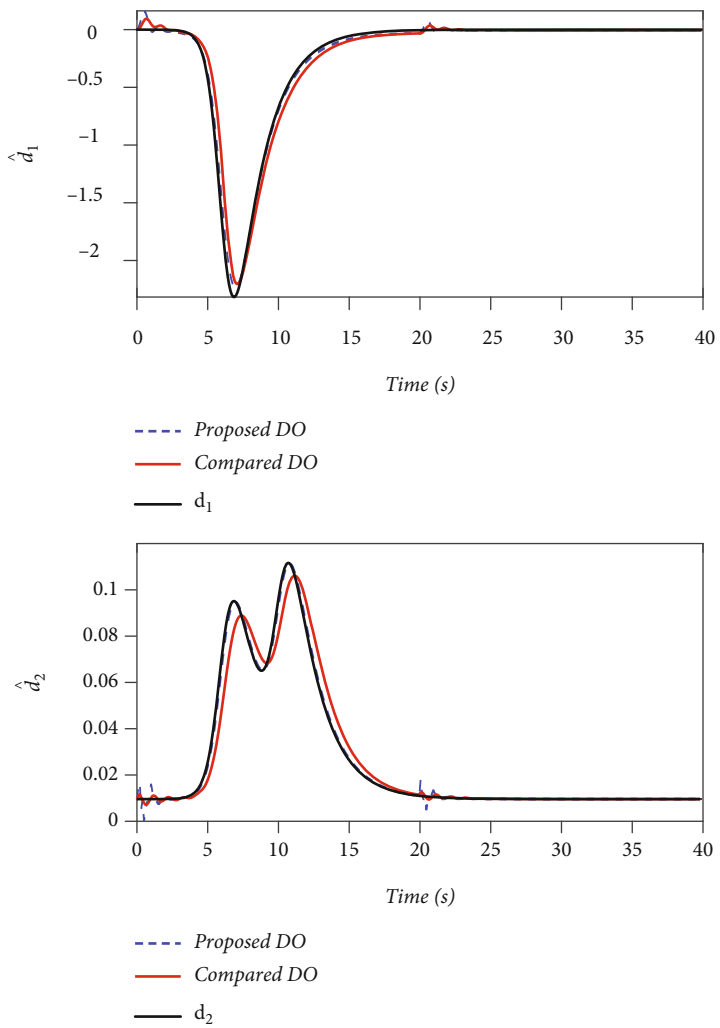

Figure 7: Estimation of d_1 and d_2.

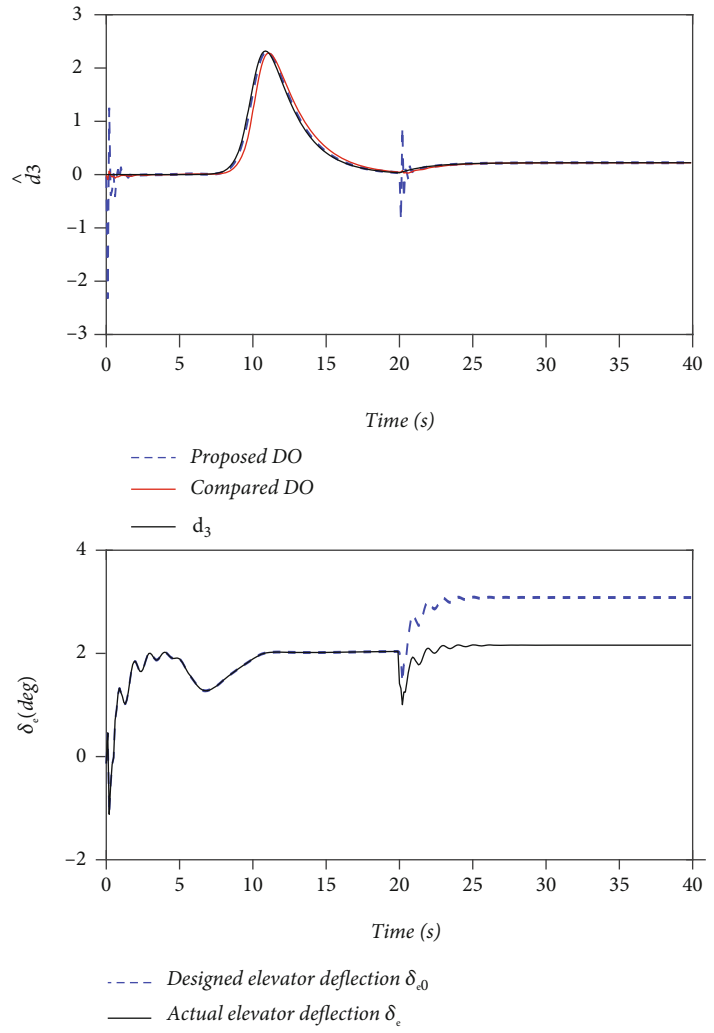

FIGURE 8: Estimation of d_3 and control input.

Naturally, it can be shown that the derivative of fixed-time filter output signal $\dot{x}_{ic}$ is bounded because of the boundedness of y_i. Then, we can get that the virtual control signal x_{id} is bounded because y_i, z_1, and $\dot{x}_{ic}$ are both bounded.

According to above analysis, one can get that V will converge to the set $\{V : V \le \sqrt{C/\mu_4}\}$ in fixed-time $T_s \le 2/\mu_3 + 1/\mu_4$. Moreover, we have that the tracking errors z_i and the filter errors $y_i i = 1, 2, 3$ will converge to the sets

$$\Omega_{z_i} = \left\{ z_i \le \sqrt{2\sqrt{\frac{C}{\mu_4}}} \right\},$$
$$\Omega_{y_i} = \left\{ y_i \le \sqrt{2\sqrt{\frac{C}{\mu_4}}} \right\}. \tag{53}$$

5. Numerical Simulations

In this section, comparative method [21] is used to verify the effectiveness of the proposed composite control scheme. The detailed parameters of the longitudinal model can refer to [27].

The controller parameters are designed as

$$\begin{aligned}
&k_{11} = k_{21} = k_{31} = 0.1, k_{12} = k_{22} = k_{32} = 0.1, \varepsilon_{z1} \\
&\quad = \varepsilon_{z2} = \varepsilon_{z3} = 0.01, k_{13} = 0.2, k_{23} = 0.7, k_{33} = 0.4, \\
&k_{f21} = 10, k_{f22} = 1, k_{f23} = 10, k_{f31} = 1, k_{f32} \\
&\quad = 0.001, k_{f33} = 10, \varepsilon_{y2} = 0.1, \varepsilon_{y3} = 0.0001, \theta_1 \\
&\quad = \theta_2 = \theta_3 = 1.1, \\
&\lambda_{11} = 10, \lambda_{12} = 0.5, \lambda_{13} = 0.5, \lambda_{21} = 10, \lambda_{22} \\
&\quad = 0.5, \lambda_{23} = 0.5, \lambda_{31} = 10, \lambda_{32} = 0.5, \gamma_1 \\
&\quad = \gamma_2 = \gamma_3 = 0.1, \\
&\lambda_{33} = 0.5, \varepsilon_1 = \varepsilon_2 = \varepsilon_3 = 0.5, \delta_1 = \delta_2 = \delta_3 \\
&\quad = 0.5, \frac{\sigma_{11}}{n_1} = \frac{\sigma_{12}}{n_2} = \frac{\sigma_{13}}{n_3} = 10, \frac{\sigma_{21}}{n_1^2} \\
&\quad = \frac{\sigma_{22}}{n_2^2} = \frac{\sigma_{23}}{n_3^2} = 0.01.
\end{aligned} \tag{54}$$

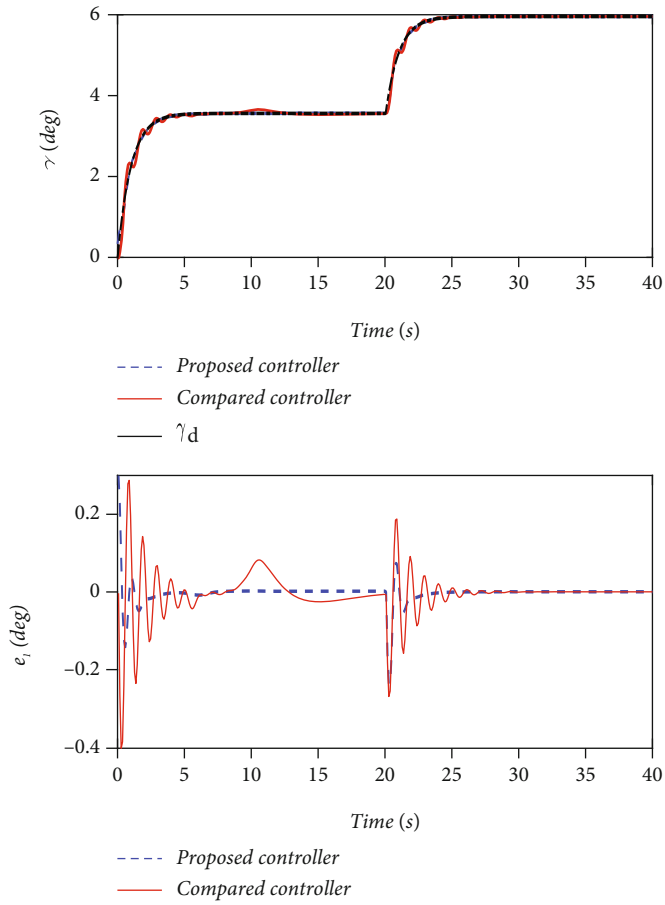

Figure 9: Tracking error e_1 and trajectories of γ.

The reference signal x_d is generated through the following filter:

$$\gamma_d(s) = \frac{5}{s+5}\gamma_d(s). \tag{55}$$

The initial state of the system is that $x_1(0) = 0, x_2(0) = 0, x_3(0) = 0$ and the disturbance signal including wind disturbance [32] is defined as

$$\Delta_\gamma = \dot{\omega}_h, \Delta_\alpha = \left(\frac{\dot{\omega}_h}{30}\right) - \left(\frac{\dot{\omega}_x}{30}\right), \Delta_q = \dot{\omega}_x, \tag{56}$$

where ω_x, ω_h are wind components.

The reference signal and actuator fault model are designed as

$$y_d = \begin{cases} 3, t < 20 \\ 5, t \geq 20 \end{cases}, \begin{cases} p_1 = 1, b_{f1} = 0, t < 20 \\ p_1 = 0.7, b_{f1} = 0.07, t \geq 20 \end{cases}. \tag{57}$$

Case 14. Against actuator fault and slight external disturbances.

In this simulation, external wind disturbances are considered to verify the robustness of the proposed composite control scheme. Figure 1 gives the wind disturbances. Figure 2 shows the estimated lumped disturbances. One can find that the compared DO and the proposed DO are both able to estimate lumped disturbances including actuator fault and external unmatched disturbances. However, the compared DO exhibits a larger disturbance estimation error. Curves of elevator deflection are shown as Figure 3. Figures 4 and 5 illustrate the tracking errors of flight-path angle, angle of attack, and pitch rate. It can be found that flight-path angle, angle of attack, and pitch rate react reasonably. The proposed controller exhibits smaller tracking errors than the compared method, when the actuator is fault at $t = 20s$.

Case 15. Against actuator fault and severe external disturbances.

In this simulation, severe wind disturbances are imposed on the UAV. The other conditions are kept as Case 14. Figure 6 gives the curves of the wind disturbances. Figures 7 and 8 illustrate the lumped disturbances estimation. Figures 9 and 10 describe the tracking errors. It can be seen that the disturbance estimation errors of the proposed DO are much smaller than the compared method. It is validated that the proposed controller operates well even though there exist the reinforced wind disturbance and actuator fault.

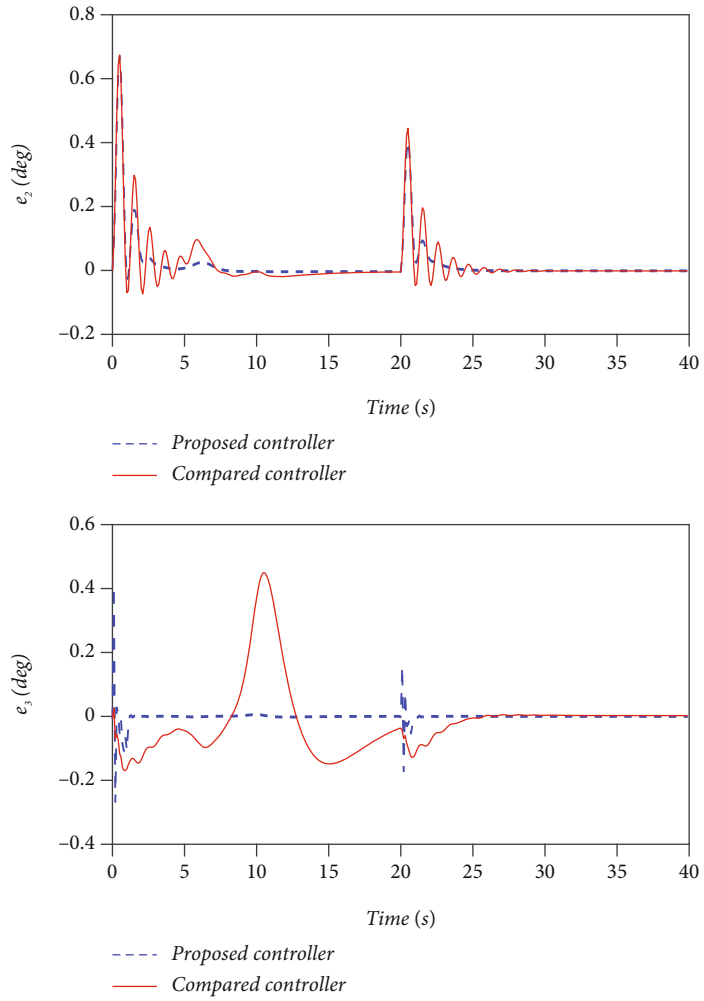

FIGURE 10: Tracking errors e_2 and e_3.

6. Conclusions

In this paper, the fixed-time fault-tolerant tracking control problem for the fixed-wing UAVs subject to external disturbances and actuator fault has been addressed. To estimate the lumped disturbance with unknown upper bound precisely, a new disturbance observer has been proposed. A new fixed-time fault-tolerant controller without fractional power terms has been proposed in this paper, which overcomes the potential singularity problem often encountered in fixed-time backstepping design procedures. Moreover, a new fixed-time dynamic surface filter has been added in the controller design to prevent the phenomenon of "differential explosion." Lyapunov stability analysis has proven the stability of the proposed control scheme. The simulation results verify the effectiveness of the proposed method.

Data Availability

The data used to support the findings of this study are included within the article.

Conflicts of Interest

The authors declare that they have no known competing financial interests or personal relationships that could have appeared to influence the work reported in this paper.

Acknowledgments

This work is supported by the National Natural Science Foundation of China (Grant no. 61903126), Key R&D and Promotion Projects in Henan Province (Grant no. 212102210197, 202102210130), the Key Scientific Research Project of Colleges and Universities in Henan Province (Grant no. 20A590001), the Outstanding Youth Fund of Henan Polytechnic University (Grant no. 722515/003/034), Outstanding Youth Fund of Henan Polytechnic University (Grant no. J2022-7), and the Doctoral Innovation Fund of Henan Polytechnic University (Grant no. 760807/028).

References

[1] Y. Xu, S. Tong, and Y. Li, "Adaptive fuzzy fault-tolerant output feedback control of uncertain nonlinear systems with actuator

faults based on dynamic surface technique," *Journal of the Franklin Institute*, vol. 350, no. 7, pp. 1768–1786, 2013.

[2] S. Gao, H. Dong, B. Ning, and X. Yao, "Single-parameter-learning-based fuzzy fault-tolerant output feedback dynamic surface control of constrained-input nonlinear systems," *Information Sciences*, vol. 385-386, pp. 378–394, 2017.

[3] H. Khebbache, S. Labiod, and M. Tadjine, "Adaptive sensor fault-tolerant control for a class of multi-input multi-output nonlinear systems: adaptive first-order filter-based dynamic surface control approach," *ISA Transactions*, vol. 80, pp. 89–98, 2018.

[4] H. Khebbache, M. Tadjine, and S. Labiod, "Adaptive sensor-fault tolerant control for a class of MIMO uncertain nonlinear systems: adaptive nonlinear filter-based dynamic surface control," *Journal of the Franklin Institute*, vol. 353, no. 6, pp. 1313–1338, 2016.

[5] Q. Lei, J. Yu, and Q. G. Wang, "Discrete-time command filtered adaptive fuzzy fault-tolerant control for induction motors with unknown load disturbances," *Journal of the Franklin Institute*, vol. 358, no. 5, pp. 2765–2779, 2021.

[6] S. Zeghlache, H. Mekki, A. Bouguerra, and A. Djerioui, "Actuator fault tolerant control using adaptive RBFNN fuzzy sliding mode controller for coaxial octorotor UAV," *ISA Transactions*, vol. 80, pp. 267–278, 2018.

[7] Z. Yu, Y. Zhang, Z. Liu, Y. Qu, C.-Y. Su, and B. Jiang, "Decentralized finite-time adaptive fault-tolerant synchronization tracking control for multiple UAVs with prescribed performance," *Journal of the Franklin Institute*, vol. 357, no. 16, pp. 11830–11862, 2020.

[8] Z. Yu, Y. Zhang, B. Jiang et al., "Distributed adaptive fault-tolerant close formation flight control of multiple trailing fixed-wing UAVs," *ISA Transactions*, vol. 106, pp. 181–199, 2020.

[9] Y. Cai, H. Zhang, J. Zhang, S. Sun, and Q. He, "Distributed fault-tolerant output regulation for heterogeneous linear multi- agent systems under actuator faults," *Journal of the Franklin Institute*, vol. 358, no. 7, pp. 3303–3331, 2021.

[10] Y. Liu, X. Dong, Z. Ren, and J. Cooper, "Fault-tolerant control for commercial aircraft with actuator faults and constraints," *Journal of the Franklin Institute*, vol. 356, no. 7, pp. 3849–3868, 2019.

[11] A. Abbaspour, P. Aboutalebi, K. K. Yen, and A. Sargolzaei, "Neural adaptive observer-based sensor and actuator fault detection in nonlinear systems: application in UAV," *ISA Transactions*, vol. 67, pp. 317–329, 2017.

[12] B. Brahmi, M. Driscoll, I. K. El Bojairami, M. Saad, and A. Brahmi, "Novel adaptive impedance control for exoskeleton robot for rehabilitation using a nonlinear time-delay disturbance observer," *ISA Transactions*, vol. 108, pp. 381–392, 2021.

[13] L. Zhang, C. Wei, R. Wu, and N. Cui, "Fixed-time extended state observer based non-singular fast terminal sliding mode control for a VTVL reusable launch vehicle," *Aerospace Science and Technology*, vol. 82-83, pp. 70–79, 2018.

[14] Y. Huang, M. Zhu, Z. Zheng, and M. Feroskhan, "Fixed-time autonomous shipboard landing control of a helicopter with external disturbances," *Aerospace Science and Technology*, vol. 84, pp. 18–30, 2019.

[15] L. Cui, X. Hou, Z. Zuo, and H. Yang, "An adaptive fast super-twisting disturbance observer-based dual closed-loop attitude control with fixed-time convergence for UAV," *Journal of the Franklin Institute*, vol. 359, no. 6, pp. 2514–2540, 2022.

[16] D. Swaroop, J. K. Hedrick, P. P. Yip, and J. C. Gerdes, "Dynamic surface control for a class of nonlinear systems," *IEEE Transactions on Automatic Control*, vol. 45, no. 10, pp. 1893–1899, 2000.

[17] Y. Hu, S. Dian, R. Guo, S. Li, and T. Zhao, "Observer-based dynamic surface control for flexible-joint manipulator system with input saturation and unknown disturbance using type-2 fuzzy neural network," *Neurocomputing*, vol. 436, pp. 162–173, 2021.

[18] X. Wu, W. Zheng, X. Zhou, and S. Shao, "Adaptive dynamic surface and sliding mode tracking control for uncertain QUAV with time-varying load and appointed-time prescribed performance," *Journal of the Franklin Institute*, vol. 358, no. 8, pp. 4178–4208, 2021.

[19] X. Yang, Y. Ge, W. Deng, and J. Yao, "Adaptive dynamic surface tracking control for uncertain full-state constrained nonlinear systems with disturbance compensation," *Journal of the Franklin Institute*, vol. 359, no. 6, pp. 2424–2444, 2022.

[20] K. Xia and H. Son, "Adaptive fixed-time control of autonomous VTOL UAVs for ship landing operations," *Journal of the Franklin Institute*, vol. 357, no. 10, pp. 6175–6196, 2020.

[21] Z. Zhang and Y. Wu, "Further results on fixed-time stabilization and tracking control of a marine surface ship subjected to output constraints," *Ieee Transactions on Systems Man Cybernetics-Systems*, vol. 51, no. 9, pp. 5300–5310, 2021.

[22] Z. Guan, H. Liu, Z. Zheng, M. Lungu, and Y. Ma, "Fixed-time control for automatic carrier landing with disturbance," *Aerospace Science and Technology*, vol. 108, article 106403, 2021.

[23] M. Zhuang, L. Tan, K. Li, and S. Song, "Fixed-time formation control for spacecraft with prescribed performance guarantee under input saturation," *Aerospace Science and Technology*, vol. 119, article 107176, 2021.

[24] Y. Tian, C. Du, P. Lu, Q. Jiang, and H. Liu, "Nonsingular fixed-time attitude coordinated tracking control for multiple rigid spacecraft," *ISA Transactions*, 2022.

[25] X. Jin, "Adaptive fixed-time control for MIMO nonlinear systems with asymmetric output constraints using universal barrier functions," *IEEE Transactions on Automatic Control*, vol. 64, no. 7, pp. 3046–3053, 2018.

[26] J. Tan, Y. Dong, P. Shao, and G. Qu, "Anti-saturation adaptive fault-tolerant control with fixed-time prescribed performance for UAV under AOA asymmetric constraint," *Aerospace Science and Technology*, vol. 120, article 107264, 2022.

[27] Z. Wu, J. Ni, W. Qian, X. Bu, and B. Liu, "Composite prescribed performance control of small unmanned aerial vehicles using modified nonlinear disturbance observer," *ISA Transactions*, vol. 116, pp. 30–45, 2021.

[28] H. Li, C.-L. Liu, Y. Zhang, and Y.-Y. Chen, "Adaptive neural networks-based fixed-time fault-tolerant consensus tracking for uncertain multiple Euler-Lagrange systems," *ISA Transactions*, 2021.

[29] S. Q. Liu and J. F. Whidborne, "Observer-based incremental backstepping sliding-mode fault-tolerant control for blended-wing-body aircrafts," *Neurocomputing*, vol. 464, pp. 546–561, 2021.

[30] L. Wei, M. Chen, and T. Li, "Disturbance-observer-based formation-containment control for UAVs via distributed adaptive event -triggered mechanisms," *Journal of the Franklin Institute*, vol. 358, no. 10, pp. 5305–5333, 2021.

[31] Z. Gao and G. Guo, "Fixed-time sliding mode formation control of AUVs based on a disturbance observer," *IEEE/CAA Journal of Automatica Sinica*, vol. 7, no. 2, pp. 539–545, 2020.

[32] C. Liu and W.-H. Chen, "Disturbance rejection flight control for small fixed-wing unmanned aerial vehicles," *Journal of Guidance, Control, and Dynamics*, vol. 39, no. 12, pp. 2810–2819, 2016.